

High-Throughput GPU Implementation of Dilithium Post-Quantum Digital Signature

Shiyu Shen^{1,4}, Hao Yang², Wangchen Dai³, Zhe Liu^{3,2}, and Yunlei Zhao^{1,4}

¹ School of Computer Science, Fudan University, Shanghai, China

² College of Computer Science and Technology, Nanjing University of Aeronautics and Astronautics, Nanjing, China

³ Research Institute of Basic Theories, Zhejiang lab, Hangzhou, China

⁴ State Key Laboratory of Cryptology, Beijing

Abstract. In this work, we present a well-optimized GPU implementation of Dilithium, one of the NIST post-quantum standard digital signature algorithms. We focus on warp-level design and exploit several strategies to improve performance, including memory pool, kernel fusing, batching, streaming, etc. All the above efforts lead to an efficient and high-throughput solution. We profile on both desktop and server-grade GPUs, and achieve up to $57.7\times$, $93.0\times$, and $63.1\times$ higher throughput on RTX 3090Ti for key generation, signing, and verification, respectively, compared to single-thread CPU. Additionally, we study the performance in real-world applications to demonstrate the effectiveness and applicability of our solution.

Keywords: Post-quantum cryptography · Digital signature · Dilithium · Parallel processing · GPU.

1 Introduction

Digital signature is a cryptographic primitive that provides message integrity and authenticity. As a fundamental building block of information security, digital signatures are widely adopted in various protocols and applications such as Transport Layer Security (TLS) and blockchain systems. Meanwhile, the rapid development of quantum computing has posed a threat to the classical signature algorithms currently in use like RSA and ECDSA. The hardness of these algorithms can be reduced to integer factorization and discrete logarithm problems, which are believed to be vulnerable to quantum attacks. Although it is unpredictable whether a sufficient powerful quantum computer can be built within decades, it is critical to study post-quantum digital signatures and their practical applications for long-term security.

The National Institute of Standards and Technology (NIST) started the standardization process in 2016 to select post-quantum signature and public-key encryption/key encapsulation mechanism (KEM) [1]. After three rounds of evaluation, NIST chose three signatures to standardize in 2022, where CRYSTALS-Dilithium [2,5] is one of them and is recommended as the primary choice. Dilithium is efficient and has strong theoretical security guarantees. Due to the advantages, it has been intensively studied for real-world applications and migrations. For example, ArielCoin⁵, an experimental digital currency, uses Dilithium for verification and authentication. The liboqs library⁶, presented by the Open Quantum Safe project, integrates Dilithium for a quantum-safe TLS protocol. However, high computational complexity and large IO transfer size of lattice-based schemes, as well as huge numbers of queries for sever-based scenarios, usually makes Dilithium a performance bottleneck. As a result, a highly optimized implementation of Dilithium with high throughput and efficient memory management for sever-based solutions is in need.

Due to the massive parallelism, GPUs are commonly applied for throughput-oriented concurrent processing of signatures. GPU-based implementations of classical signatures and post-quantum KEMs with high performance have been deeply studied [7–10,13]. However, there are few works that focus on post-quantum signatures [11,12]. Previous works use a single thread [8] or partial threads in a warp [7] to execute a task. This is not suitable for hiding IO latency, as data accesses may not be coalesced. The implementations of

⁵ <https://github.com/ArielCoinOrg>

⁶ <https://github.com/open-quantum-safe/liboqs>

Dilithium on software [4, 5] and hardware [3, 14] platforms have been studied, but they focus on compact design and are not sufficient to meet the throughput and real-time requirements.

Contributions. In this work, we present a well-optimized GPU implementation of Dilithium, featuring high throughput and memory efficiency. In summary, we make the following contributions:

- For all operations, we devise a warp-based implementation to improve throughput. We exploit CUDA integer intrinsics and warp-level primitives to enable parallel computing of massive sequential operations. Benefiting from this approach, the data accesses are coalesced and the workload of threads are consistent, thus providing low IO latency and high performance.
- We propose several optimizations for performance and memory usage, including on-the-fly computing, kernel fusing, etc. We implement a warp-based memory pool to provide efficient memory management. Based on kernel profiling, we obtain the optimal strategy for resource consumption per block, which yields the highest occupancy of streaming multiprocessors.
- We study the approaches to process and schedule concurrent key generation, signing and verification tasks, including batching, streaming and workload partition. We provide a comparison under different circumstances.
- We implemented our design on both desktop and server-grade GPU for a proof-of-concept study. Compared to CPU baseline, we improve the throughput by up to 85.6 \times , 129.9 \times , and 92.4 \times for the three procedures on the 3090Ti GPU. Additionally, we offer a study case of our implementation in ArielCoin.

2 Preliminaries

2.1 Notation

Let \mathbb{Z} be the group of integers. For a prime q , we define $\mathbb{Z}_q := \mathbb{Z} \cap [-q/2, q/2)$. Let n be a 2-power integer, we use $R = \mathbb{Z}[X]/(X^n + 1)$ to denote the $2n$ -th cyclotomic ring and $R_q = R/qR$ to denote the residue ring modulo q . We use lower-case letters to indicate ring elements (polynomials) like $f = \sum_{i=0}^{n-1} f_i X^i$. The vectors and matrices of polynomials are represented in bold lower-case (e.g., \mathbf{v}) and upper-case letters (e.g., \mathbf{A}), respectively. The “hat” symbol indicates elements in NTT domain. The $\text{mod}^{\pm}\alpha$ denote the centered reduction modulo α that outputs representatives in range $(-\lfloor \frac{\alpha+1}{2} \rfloor, \lfloor \frac{\alpha}{2} \rfloor]$. We denote the ℓ_{∞} -norm as $\|\cdot\|_{\infty}$ and use $[\cdot]$ to record the coefficient numbers that equal to 1. The notation $\{0, 1\}^l$ (resp., $\{0, 1\}^*$) indicates an l -bit stream (resp., arbitrary length), and $|\cdot|$ is the bit-length. The operator \parallel converts elements as bit streams implicitly and concatenates them. For a finite set S , $a \leftarrow S$ refers to uniform sampling from S . We define $S_{\eta} := \{\omega : \omega \in R, \|\omega\|_{\infty} \leq \eta\}$ and $\tilde{S}_{\eta} := \{\omega \text{ mod }^{\pm} 2\eta : \omega\}$. The operator $\llbracket \mathcal{P} \rrbracket$ returns 1 if \mathcal{P} is true and 0 otherwise.

2.2 CRYSTALS-Dilithium

Dilithium is a lattice-based digital signature scheme, which has security proof in the QROM under the Module Learning With Errors (MLWE) and a variant of Module Short Integer Solution (MSIS) assumptions [2, 5]. The scheme consists of three procedures: key generation (**Gen**), signing (**Sign**) and verification (**Verify**), specified in Algorithm 1, 2 and 3, respectively. Table 1 presents the parameters of Dilithium corresponding to three NIST security levels.

Table 1: Parameter specifications of Dilithium for three NIST security levels

Level	n	q	(k, l)	d	τ	γ_1	γ_2	η	β	ω	L_1	L_2
2	256	8380417	(4,4)	13	39	2^{17}	95232	2	78	80	256	512
3	256	8380417	(6,5)	13	49	2^{19}	261888	4	196	55	256	512
5	256	8380417	(8,7)	13	60	2^{19}	261888	2	120	75	256	512

Algorithm 1 Dilithium.Gen()

- 1: $\zeta \leftarrow \{0, 1\}^{L_1}$
- 2: $(\rho, \rho', K) \in \{0, 1\}^{L_1} \times \{0, 1\}^{L_2} \times \{0, 1\}^{L_1} := \mathcal{H}(\zeta)$
- 3: $\hat{\mathbf{A}} \in R_q^{k \times \ell} := \text{ExpandA}(\rho)$
- 4: $(\mathbf{s}_1, \mathbf{s}_2) \in S_\eta^\ell \times S_\eta^k := \text{ExpandS}(\rho')$
- 5: $\mathbf{t} := \text{INTT}(\hat{\mathbf{A}} \cdot \text{NTT}(\mathbf{s}_1)) + \mathbf{s}_2$
- 6: $(\mathbf{t}_1, \mathbf{t}_0) := \text{Power2Round}_q(\mathbf{t}, d)$
- 7: $tr \in \{0, 1\}^{L_1} := \mathcal{H}(\rho \parallel \mathbf{t}_1)$
- 8: **return** $(pk = (\rho, \mathbf{t}_1), sk = (\rho, K, tr, \mathbf{s}_1, \mathbf{s}_2, \mathbf{t}_0))$

Algorithm 2 Dilithium.Sign($sk, M \in \{0, 1\}^*$)

- 1: $\mu \in \{0, 1\}^{L_2} := \mathcal{H}(tr \parallel M); \rho' \in \{0, 1\}^{L_2} := \mathcal{H}(K \parallel \mu)$
- 2: $\hat{\mathbf{A}} \in R_q^{k \times \ell} := \text{ExpandA}(\rho); \kappa := 0; (\mathbf{z}, \mathbf{h}) := \perp$
- 3: $\hat{\mathbf{s}}_1 := \text{NTT}(\mathbf{s}_1); \hat{\mathbf{s}}_2 := \text{NTT}(\mathbf{s}_2); \hat{\mathbf{t}}_0 := \text{NTT}(\mathbf{t}_0)$
- 4: **while** $(\mathbf{z}, \mathbf{h}) = \perp$ **do**
- 5: $\mathbf{y} \in S_{\gamma_1}^\ell := \text{ExpandMask}(\rho', \kappa)$
- 6: $\mathbf{w} := \text{INTT}(\hat{\mathbf{A}} \cdot \text{NTT}(\mathbf{y})); \mathbf{w}_1 := \text{HighBits}_q(\mathbf{w}, 2\gamma_2)$
- 7: $\tilde{c} \in \{0, 1\}^{256} := \mathcal{H}(\mu \parallel \mathbf{w}_1)$
- 8: $c \in B_r := \text{SampleInBall}(\tilde{c}); \hat{c} := \text{NTT}(c)$
- 9: $\mathbf{z} := \mathbf{y} + \text{INTT}(\hat{c} \cdot \hat{\mathbf{s}}_1)$
- 10: $\mathbf{v}_s := \text{INTT}(\hat{c} \cdot \hat{\mathbf{s}}_2); \mathbf{r}_0 := \text{LowBits}_q(\mathbf{w} - \mathbf{v}_s, 2\gamma_2)$
- 11: **if** $\|\mathbf{z}\|_\infty \geq \gamma_1 - \beta$ **or** $\|\mathbf{r}_0\|_\infty \geq \gamma_2 - \beta$ **then** $(\mathbf{z}, \mathbf{h}) := \perp$
- 12: **else**
- 13: $\mathbf{v}_t := \text{INTT}(\hat{c} \cdot \hat{\mathbf{t}}_0)$
- 14: $\mathbf{h} := \text{MakeHint}_q(-\mathbf{v}_t, \mathbf{w} - \mathbf{v}_s + \mathbf{v}_t, 2\gamma_2)$
- 15: **if** $\|\mathbf{v}_t\|_\infty \geq \gamma_2$ **or** $\lceil \mathbf{h} \rceil > \omega$ **then** $(\mathbf{z}, \mathbf{h}) := \perp$
- 16: $\kappa := \kappa + \ell$
- 17: **return** $\sigma = (\tilde{c}, \mathbf{z}, \mathbf{h})$

Algorithm 3 Dilithium.Verify(pk, M, σ)

- 1: $\hat{\mathbf{A}} \in R_q^{k \times \ell} := \text{ExpandA}(\rho)$
- 2: $\mu \in \{0, 1\}^{512} := \mathcal{H}(\mathcal{H}(\rho \parallel \mathbf{t}_1) \parallel M)$
- 3: $c \in B_r := \text{SampleInBall}(\tilde{c}); \hat{c} := \text{NTT}(c)$
- 4: $\mathbf{v} := \text{INTT}(\hat{\mathbf{A}} \cdot \text{NTT}(\mathbf{z}) - \hat{c} \cdot \text{NTT}(\mathbf{t}_1 \cdot 2^d))$
- 5: $\mathbf{w}'_1 := \text{UseHint}_q(\mathbf{h}, \mathbf{v}, 2\gamma_2)$
- 6: **return** $\lceil \|\mathbf{z}\|_\infty < \gamma_1 - \beta \rceil \& \lceil \tilde{c} = \mathcal{H}(\mu \parallel \mathbf{w}'_1) \rceil \& \lceil \lceil \mathbf{h} \rceil \leq \omega \rceil$

Sampling Dilithium exploits SHAKE-128/256 [6] as the extendable-output function (XOF) to extend the input seeds to sufficient random bytes and instantiates \mathcal{H} with SHAKE-256. The *rejection sampling* mechanism is applied to generate sequences that follow uniform distribution, which selects $|\mathcal{B}|$ bits per sample and only stores those less than \mathcal{B} . Through this, the `ExpandA` outputs matrix $\hat{\mathbf{A}}$ with coefficients in $[0, q)$, the `ExpandS` and `ExpandMask` generate vectors with coefficients in $[-\eta, \eta]$ and $[-\gamma_1 + 1, \gamma_1]$ respectively, and the `SampleInBall` outputs a polynomial c with τ nonzero coefficients.

Number Theoretic Transform (NTT) One major performance bottleneck is polynomial multiplication, where NTT is commonly utilized to reduce the computational complexity from $\mathcal{O}(n^2)$ to $\mathcal{O}(n \log n)$. For polynomials $f, g \in R_q$, the forward negacyclic NTT is formulated as $\hat{f} := \text{NTT}(f)$, $\hat{f}_j = \sum_{i=0}^{n-1} f_i \psi^{(2i+1)j} \pmod{q}$, and the inverse is $f := \text{INTT}(\hat{f})$, $f_i = \frac{1}{n} \sum_{j=0}^{n-1} \hat{f}_j \psi^{-(2i+1)j} \pmod{q}$, where ψ is the primitive $2n$ -th root of unity. With this technique, the multiplication is performed as $fg := \text{INTT}(\text{NTT}(f) \cdot \text{NTT}(g))$.

Bits Extraction and Hints The `Power2Round $_q(a, d)$` splits an integer a into $(a_0, a_1) := (a \bmod \pm 2^d, (a - a_0)/2^d)$. The `LowBits $_q(r, \alpha)$` and `HighBits $_q(r, \alpha)$` extract the high- and low-order bits r_1 and r_0 . By judging $\mathcal{P} := (r - r_0 = q - 1)$ where $r_0 := (r \bmod +q) \bmod \pm\alpha$, the outputs are $(r_1, r_0) := (0, r_0 - 1)$ if \mathcal{P} is true, and $(r_1, r_0) := ((r - r_0)/\alpha, r_0)$ otherwise. The `MakeHint $_q(z, r, \alpha)$` computes $r_1 := \text{HighBits}_q(r, \alpha)$ and $z_1 := \text{HighBits}_q(r + z, \alpha)$ and returns $\llbracket r_1 \neq z_1 \rrbracket$. The `UseHint $_q(h, r, \alpha)$` computes $m := (q - 1)/\alpha$ and extracts (r_1, r_0) , and outputs r_1 if $h = 0$, otherwise outputs $(r_1 + 1) \bmod +m$ if $r_0 > 0$ and $(r_1 - 1) \bmod +m$ if $r_0 \leq 0$. All above algorithms can extend to ring elements by applying coefficient-wisely.

2.3 GPU Basics

Fig. 1 presents the architecture and computational model. GPUs contain various types of memory, including registers, constant memory, shared memory (SMEM), global memory (GMEM), etc. Threads in a block have private registers and can access the SMEM. The GMEM is accessible to all threads but has the highest IO latency. During execution, the blocks are assigned to the streaming multiprocessors (SM), and every 32 threads are grouped into a warp for parallel processing.

CUDA offers several warp-level primitives. For threads in a warp, *warp shuffle* functions enable synchronized exchange of register data, which is faster than exchanging through the SMEM. *Warp vote* functions allow combining a value of each thread in a tree-reduction pattern and broadcasting the result.

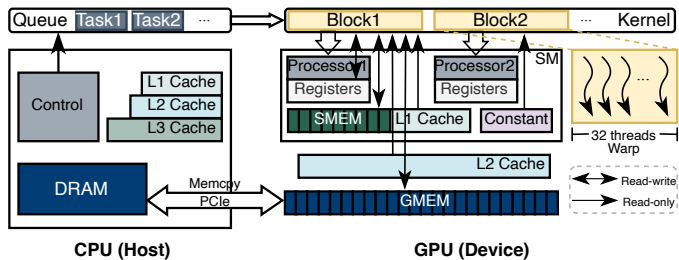


Fig. 1: The architecture and host-device computational model.

3 Implementation Details and Optimizations

In this section, we provide the pertinent details of our GPU implementation, optimizations for performance and memory usage, and approaches for task scheduling. We propose warp-based approaches for both operations and memory pool to achieve high throughput and well memory management. In our solution, we

treat a key generation, signing, and verification as a task, and one warp is responsible for a task. Each block instantiates only one warp, each kernel batches more than one block, and therefore, multiple tasks are processed during each kernel launch. This leads to better performance gain compared to other methods [7,8], as our design can coalesce data accesses and greatly reduce the IO latency.

3.1 Acceleration of Operations in Dilithium

Generally, the operations in Dilithium can be classified into three types: stream manipulation, sampling and arithmetic. However, the first type is bit-level processing and the second consists mainly of sequential computation, which are difficult for parallel computing. Additionally, the performance is also bottlenecked by the polynomial multiplication. In the following, we describe the details to overcome these challenges.

Stream Manipulation. Keeping the computational flow of threads consistent is an important point in accelerating this operation. We set the number of bits processed per iteration according to the least common multiple of the warp size, and then each thread gets the coefficient by logical shifting. The bit-shift number is obtained based on the thread’s index. In this case, no warp-divergence will occur, thus ensuring the maximum parallelism of the warp.

Parallelizing Sequential Computations. A major challenge in accelerating Dilithium is to parallelize massive sequential computations such as the rejection sampling (i.e., comparing with a bound) and number counting (i.e., comparing with 1), where the behavior of the current thread depends on the results of previous ones. However, data-dependent conditional computation and unbalanced workload lead to threads within a warp to diverge, resulting in performance degradation. We utilize the CUDA integer intrinsics and warp-level primitives to alleviate this problem and ensure that all threads compute the same task. Specifically, we set a predicate argument in each thread to record the comparison result, so that the entire state of the warp can be obtained through warp voting. If all 32 arguments are valid like Fig. 2a, no additional computation is required. Otherwise, each thread computes the local inclusive state by integer intrinsic function to get the offset of the write address as in Fig. 2b. As only the local counter of the last thread captures the correct total number, we use warp shuffle synchronization to broadcast it to all threads to ensure the correctness in the next iteration.

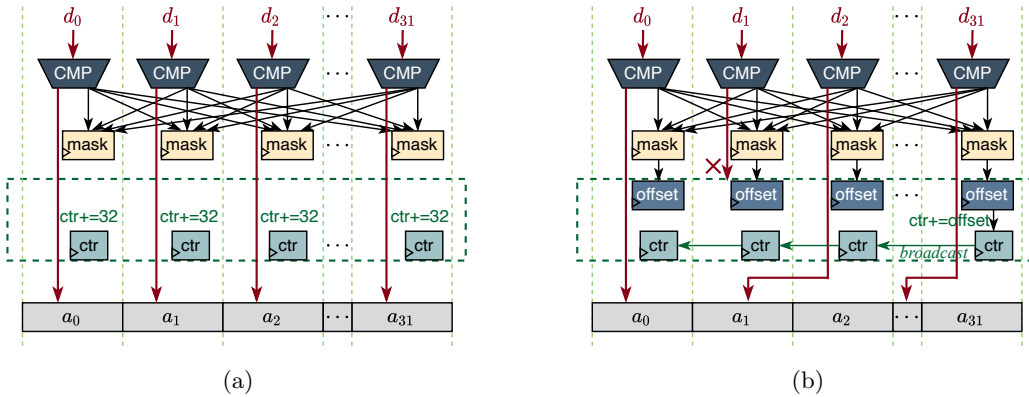


Fig. 2: Computations in rejection sampling and number counting. Note that number counting does not need to write d_i .

Note that prior work [11] precomputes a look-up table to record the positions of rejected values, and then replace the rejection sampling in the signing and verification by loading elements directly based on the table.

This approach mitigates the problem at the cost of increasing memory overhead, but it introduces additional inputs of the table and requires to transfer it to verifier along with the public key and signature. This does not follow the original design intention of Dilithium that aims at reducing communication bandwidth, and may cause incompatibility in applications.

Fast Polynomial Multiplication. We apply the negacyclic NTT with the combination of Cooley-Tukey and Gentleman-Sande algorithms follow [2] to accelerate polynomial multiplication, where transforming a n -dimension polynomial requires $\log n$ levels. As Dilithium fixes the dimension to $n = 256$, we implement a in-place constant-time 8-level NTT/INTT. In detail, each thread loads 8 coefficients into the registers and performs a radix-8 (I)NTT, which forms a coalescent 3-level processing. Then, we utilize the SMEM for fast data exchange and access the elements required by the following three levels. Throughout the computation, we only need data transfers between SMEM and registers at levels 0, 3, and 6, where the loaded elements at level i to each thread are at an interval of $2^{\log n - i - 1}$.

3.2 Memory Management

We implement a warp-based memory pool mechanism. The main consideration is to provide fast and safe memory access for explicit warp-level processing, which is our target throughout this work. For both signing and verification, we carefully adjust the order of elements following the flow of Hash functions to make the addresses of input byte streams contiguous, as shown in Fig. 3. This mechanism reduces the cost of a large amount of memory allocation and deallocation during computation. Additionally, we apply the pitch allocation to allocate linear memory to store the seeds and streams, thus fulfilling the alignment requirements.

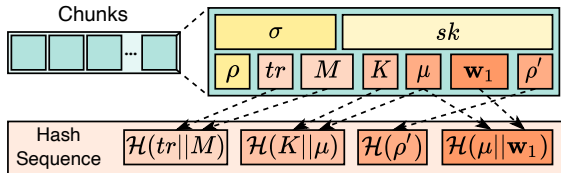


Fig. 3: The implemented warp-level memory pool (example in Sign) that stores the elements needed in a warp processing.

3.3 Optimizations for Performance and Memory Usage

We propose several methods to optimize the performance and memory usage. Specifically, we pad the memory to ensure conflict-free memory request, and reduce the memory usage and data transfer through on-the-fly computing and kernel fusing. Meanwhile, we optimize the resource consumption of each block to provide the optimal SM occupancy.

Avoid Bank Conflict. Stride SMEM accesses can lead to bank conflict and therefore decrease throughput, which exist in cases that a thread assesses several elements with consecutive addresses. For example, a thread loads 8 continuous coefficients in the first level of INTT, resulting in 8-way conflict. For best performance, we pad the memory appropriately to eliminate such memory access patterns. Fig. 4 gives an example of our solution to 2-way conflict, which also works for some other cases.

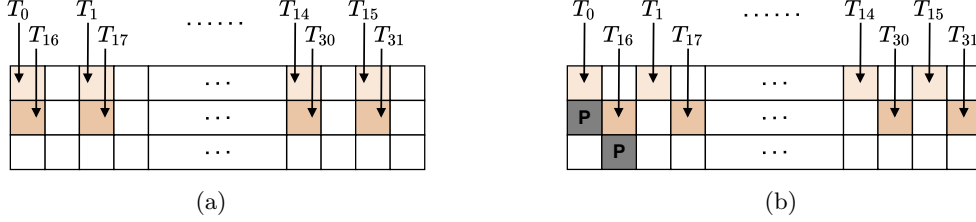


Fig. 4: (a) Example of 2-way bank conflict; (b) using memory padding to ensure conflict-free memory requests.

On-the-fly Computing. Since the multiplication with $\hat{\mathbf{A}}$ is performed only once in the **Gen** and **Verify**, storing the entire matrix is not necessary, which has high memory consumption. Therefore, we adjust the computational flow of matrix-vector multiplication to an on-the-fly manner by not storing the entire matrix or vector to reduce the memory usage. As shown in Fig. 5, instead of the traditional row-major sampling, we generate $\hat{\mathbf{A}}$ in the order of columns. Specifically, we first sample the polynomials $s_{1,j}$ and $a_{i,j}$, and then compute $a_{i,j} \cdot s_{1,j}$, $i \in [0, k), j \in [0, l)$. During processing, we only allocate one buffer as an accumulator to store k polynomials, i.e., the accumulation results. With this approach, we eliminate $2(k+1)ln$ GMEM accesses and reduce the storage requirements from $(k+1)ln$ to kn of this process.

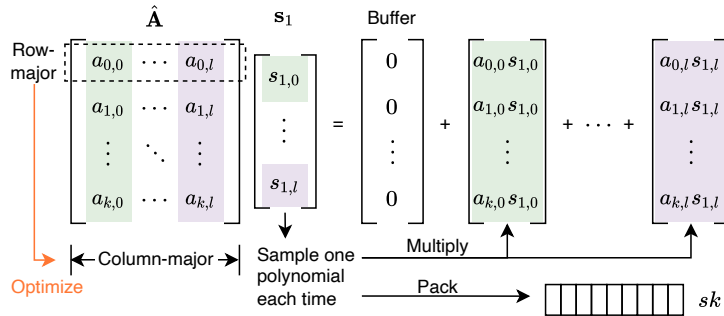


Fig. 5: Optimized matrix-vector multiplication with less memory requirement.

Kernel Fusing Despite accelerating each operation separately is straightforward, it neglects the correlation between operations and introduces much kernel launching and data transfer overhead. Since the operations in Dilithium have both internal and external data dependencies, we adapt the operations and fuse the kernels. This technique allows us to keep data in registers and SMEM, which offer relatively low IO latency. Therefore, we can reuse them to reduce data access.

In our implementation, we fuse the entire **Gen**, the while loop in **Sign**, and the **Verify** into one kernel, respectively. Specifically, the fusion of the four judgments in the while loop is shown in Fig. 6. During the processing, the next computation is entered only when the ℓ_∞ -norm of the currently judged element is within the preset threshold. We make the ℓ_∞ -norm checking function well compatible to the arithmetic operations. Thus, in each iteration, we immediately check the 32 coefficients when they are generated by the warp. With this technique, we can provide a more timely rejection.

Improving SM Occupancy The SM occupancy reflects the utilization of GPU hardware ability. Although SMEM and register files provide faster access speed, excessive use of them in a block will reduce the SM occupancy, because these resources are shared by blocks assigned to an SM. This may decrease the number

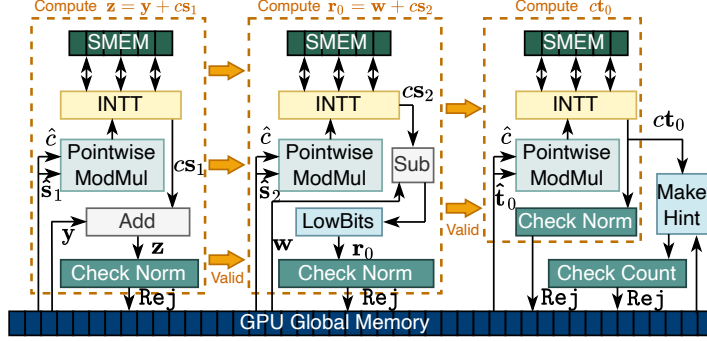


Fig. 6: Logical flow and data access pattern in Sign.

of active warps and reduce the throughput. To strike a balance between IO latency and SM occupancy, we adjust the SMEM usage in each block carefully and test the corresponding performance. Based on the kernel profiling and experimental results, we only allocate SMEM to store the rejection flag Rej , the seeds to make addresses contiguous, and two buffers to store intermediate polynomials, leaving other elements in GMEM. Meanwhile, each block is instantiated with one warp. Although storing frequently used elements like \hat{c} in SMEM provides a faster access speed, storing in GMEM and caching them provides a better alternative, which shows higher theoretical occupancy and better performance.

3.4 Batching and Streaming Multiple Tasks

Using a block with one warp to process a signing or verification task leaves much hardware resources for batching multiple computational tasks in a kernel. We consider the following methods to execute multiple tasks concurrently:

- *Batching in a kernel.* We set the number of blocks in a kernel to the number of tasks, where all kernels are executed on the default CUDA stream.
- *Streaming.* Compared to the previous method, we reduce the number of tasks batched in a kernel and then launch multiple streams to execute the kernels.
- *GPU-CPU workload partition.* Assigning the tasks to the GPU and CPU and make both compute together.

The effectiveness of the three methods varies on GPUs with different computing capabilities, and may be affected by factors such as the rejection numbers of Sign. A detailed comparison is presented in Section 4.2.

4 Performance Evaluation

4.1 Experimental Setup

We compile the C/C++ and GPU implementations with g++ 12.2.0 and CUDA 11.8 on Arch Linux with kernel 5.15. We deploy our implementation on two GPUs, i.e., a NVIDIA GeForce RTX 3090Ti and a NVIDIA Tesla V100S PCIe. The performance of the CPU baseline is obtained on an Intel(R) Core(TM) i9-12900KS CPU with 16 cores.

4.2 Performance

In the following, we present the performance of our GPU implementation, the performance gains with our optimization techniques, and the comparisons with CPU implementations and other works. Additionally, we compare different methods to achieve task-level parallelism under various configurations.

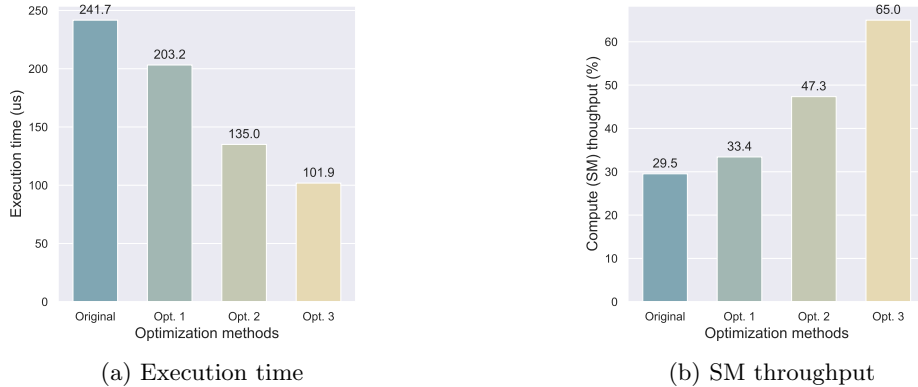


Fig. 7: Impact of the proposed optimizations.

Speedup Breakdown. We choose the computation of $\hat{\mathbf{t}}_0$ as an example to show the impact of the proposed optimizations in this work. This process consists of unpacking from the secret key to get \mathbf{t}_0 and then computing $\text{NTT}(\mathbf{t}_0)$. Below is the original implementation and our step-by-step optimizations. Fig. 7 presents the speedups and SM throughput results.

- Original: we launch an unpacking kernel and store \mathbf{t}_0 in GMEM, and then launch another kernel for NTT.
- Opt. 1: first, we apply kernel fusing to fuse the two kernels. This brings 15.9% speedup and 13.2% improvement for the SM throughput.
- Opt. 2: second, due to Opt. 1 we can merge the loops in unpacking and NTT and use registers to store intermediate values. Considering the SM occupancy, we only use an n -length SMEM for NTT. This reduces 33.6% execution time and improves SM throughput by 41.6%.
- Opt. 3: third, we pad the n -length SMEM to avoid bank conflict. Owing to the optimizations, we improve the original runtime by $2.4\times$ and the SM throughput by $2.2\times$.

Comparisons of Streaming and Batching. Fig. 8 provides a comparison of the different methods for concurrent processing. In Fig. 8a and 8b, when the GPU hardware resources are fully utilized, the amortized time for a task tends to be stable. Because using multiple streams is better at hiding the IO latency of data transfer between the CPU and GPU, this shows better performance compared to batching in our experiments. In Fig. 8c and 8d, we present the performance of executing 8192 tasks with different stream numbers. Because of the uncertainty in the `Sign`, i.e., the rejection numbers, it has fluctuations at first, and choosing 10 streams is more appropriate in general. When the computation is asynchronous, using workload partition may further improve performance because this method makes full use of the CPU.

Performance of Scheme. In Table 2, we list the performance for the Dilithium scheme of our implementation and the comparisons. The results of C and AVX2 implementations are obtained by running the official implementation⁷ on our platform. The work [11] is closed-source, so we use the results in the paper that obtained on a Jetson AGX Xavier GPU. We recall that in [11] the authors replace the most time-consuming rejection sampling with simple loading data based on known positions. This is inappropriate and may cause incompatibility in applications, as illustrated in Sec 3.1. The work [4] and [14] are the state-of-the-art Neon-based implementation and FPGA design of Dilithium. The results we list come from the original paper. For our GPU implementation without WP, we report the performance of the method using 10 streams, which

⁷ <https://github.com/pq-crystals/dilithium>

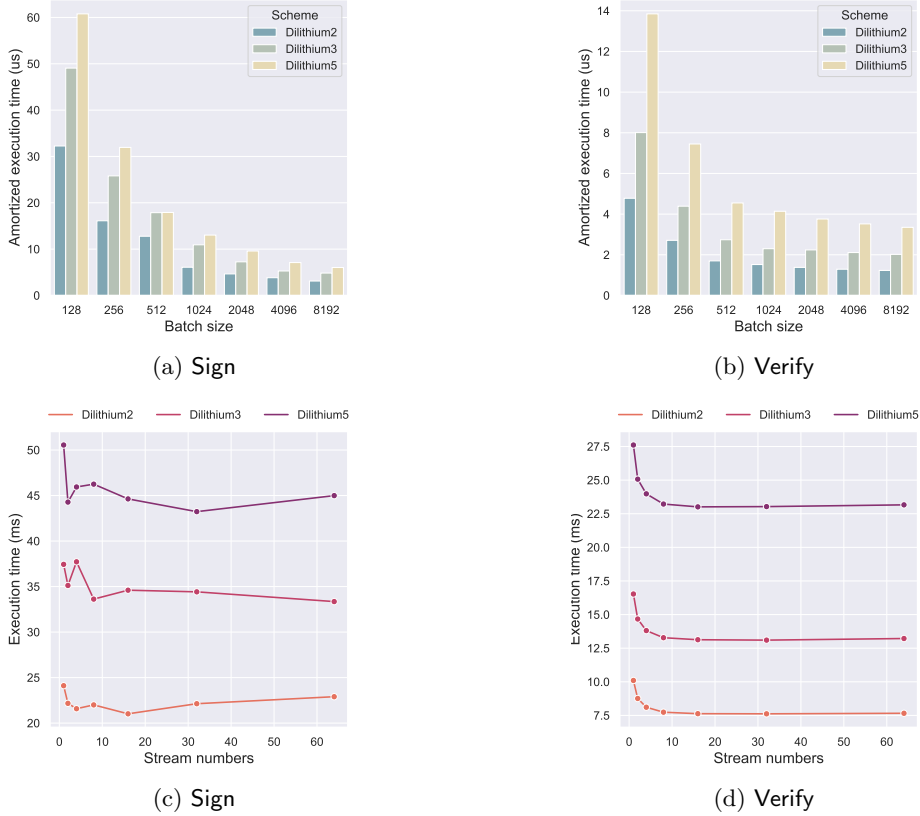


Fig. 8: Execution time of batching multiple tasks in (a) Sign and (b) Verify, and processing 8192 tasks with different stream numbers in (c) Sign and (d) Verify.

Table 2: Throughput of C and AVX2 implementations on CPU, our implementations with and without workload partition (WP), and related works on GPU [11], ARM Cortex-A72 [4], and FPGA [14]. The metric is the operations per second (OP/s). The speedup refers to the comparison between 3090Ti and CPU baseline.

Level	Procedure	CPU		Our work (without WP)			Our work (with WP)			Related Works		
		Baseline	AVX2	V100S	3090Ti	Speedup	V100S	3090Ti	Speedup	[11]	[4]	[14]
2	Gen	22,871	70,997	126,002	1,258,102	55.0×	167,921	1,881,193	82.3×	84,993	5,561	23,217
	Sign	5,520	24,719	41,486	513,125	93.0×	52,209	717,306	129.9×	33,965	2,310	3,448
	Verify	21,220	67,451	128,045	1,339,569	63.1×	189,686	1,960,182	92.4×	67,738	5,498	21,904
3	Gen	12,092	41,754	68,164	697,627	57.7×	90,960	1,035,046	85.6×	51,099	2,908	16,555
	Sign	3,288	15,575	30,495	304,798	92.7×	37,901	427,174	129.9×	14,875	1,377	2,167
	Verify	13,193	42,187	73,010	777,054	58.9×	108,318	1,141,073	86.5×	44,502	3,352	15,671
5	Gen	8,504	26,281	41,142	425,906	50.1×	54,904	632,489	74.4×	31,800	1,916	11,051
	Sign	2,703	12,719	23,376	232,507	86.0×	30,391	329,545	121.9×	20,396	1,044	1,977
	Verify	8,047	26,705	40,937	443,856	55.2×	60,796	643,110	79.9×	27,511	1,961	10,716

shows better results than batching. Compared with the CPU baseline, our implementation shows $50.1\times$ - $57.7\times$ improvement for **Gen**, $86.0\times$ - $93.0\times$ improvement for **Sign**, and $55.2\times$ - $63.1\times$ improvement for **Verify**. Since the computation is asynchronous, we partition part of the workload to the CPU. The CPU executes a multi-threaded AVX2 implementation, which we implement based on the open-source code, and we use all 24 threads of the CPU. With this WP technique, we obtain up to $85.6\times$, $129.9\times$, and $92.4\times$ improvements for the three procedures on the 3090Ti GPU, respectively.

4.3 Case Study in ArielCoin

ArielCoin is the first cryptocurrency to use Dilithium for signature to enable post-quantum safe smart contracts and non-fungible token marketplace. Based on our testing of the source code, the signature verification is executed roughly 3400 times per minute on average and consumes 6.57% of the total runtime. Using our implementation, the time of this process can be reduced by 98.3%. Currently, there are more than 370 thousand blocks, which contain plenty of transactions and signatures. Our solution can alleviate the bottlenecks and can achieve better speedups in larger scale applications like many existing cryptocurrencies, which are considering the threat of quantum attacks.

5 Conclusion

In this work, we present a high-throughput GPU implementation of Dilithium, a post-quantum digital signature scheme, and show our solutions to optimize the performance, memory usage, and process multiple tasks. The experimental results demonstrate that our implementation is able to provide an efficient and quantum-resistant solution for applications.

References

1. Alagic, G., Apon, D., Cooper, D., Dang, Q., Dang, T., Kelsey, J., Lichtinger, J., Miller, C., Moody, D., Peralta, R.: Status report on the third round of the nist post-quantum cryptography standardization process. US Department of Commerce, NIST (2022)
2. Bai, S., Ducas, L., Kiltz, E., Lepoint, T., Lyubashevsky, V., Schwabe, P., Seiler, G., Stehlé, D.: Crystals-dilithium: Algorithm specifications and supporting documentation. Submission to the NIST's post-quantum cryptography standardization process (2020)
3. Banerjee, U., Ukyab, T.S., Chandrakasan, A.P.: Sapphire: A configurable crypto-processor for post-quantum lattice-based protocols. *IACR Transactions on Cryptographic Hardware and Embedded Systems* **2019**(4), 17–61 (2019). <https://doi.org/10.13154/tches.v2019.i4.17-61>
4. Becker, H., Hwang, V., Kannwischer, M.J., Yang, B.Y., Yang, S.Y.: Neon ntt: Faster dilithium, kyber, and saber on cortex-a72 and apple m1. *IACR Transactions on Cryptographic Hardware and Embedded Systems* **2022**(1), 221–244 (2022). <https://doi.org/10.46586/tches.v2022.i1.221-244>
5. Ducas, L., Kiltz, E., Lepoint, T., Lyubashevsky, V., Schwabe, P., Seiler, G., Stehlé, D.: Crystals-dilithium: A lattice-based digital signature scheme. *IACR Trans. Cryptogr. Hardw. Embed. Syst.* **2018**(1), 238–268 (2018)
6. Dworkin, M.J., et al.: Sha-3 standard: Permutation-based hash and extendable-output functions (2015)
7. Gao, Y., Xu, J., Wang, H.: cunh: Efficient gpu implementations of post-quantum kem newhope. *IEEE Transactions on Parallel and Distributed Systems* **33**(3), 551–568 (2022). <https://doi.org/10.1109/tpds.2021.3097277>
8. Gupta, N., Jati, A., Chauhan, A.K., Chattopadhyay, A.: Pqc acceleration using gpus: Frodokem, newhope, and kyber. *IEEE Transactions on Parallel and Distributed Systems* **32**(3), 575–586 (2021). <https://doi.org/10.1109/tpds.2020.3025691>
9. Lee, W.K., Seo, H., Zhang, Z., Hwang, S.O.: Tensorcrypto: High throughput acceleration of lattice-based cryptography using tensor core on gpu. *IEEE Access* **10**, 20616–20632 (2022). <https://doi.org/10.1109/access.2022.3152217>
10. Ono, T., Bian, S., Sato, T.: Automatic parallelism tuning for module learning with errors based post-quantum key exchanges on gpus. In: *2021 IEEE International Symposium on Circuits and Systems (ISCAS)*. pp. 1–5 (2021). <https://doi.org/10.1109/iscas51556.2021.9401575>

11. Seo, S.C., An, S.W.: Parallel implementation of crystals-dilithium for effective signing and verification in autonomous driving environment. *ICT Express* (2022). <https://doi.org/https://doi.org/10.1016/j.ict.2022.08.003>
12. Sun, S., Zhang, R., Ma, H.: Efficient parallelism of post-quantum signature scheme sphincs. *IEEE Transactions on Parallel and Distributed Systems* **31**(11), 2542–2555 (2020). <https://doi.org/10.1109/tpds.2020.2995562>
13. Wan, L., Zheng, F., Fan, G., Wei, R., Gao, L., Wang, Y., Lin, J., Dong, J.: A novel high-performance implementation of crystals-kyber with ai accelerator. In: *Computer Security - ESORICS 2022*. pp. 514–534. *Lecture Notes in Computer Science* (2022). https://doi.org/10.1007/978-3-031-17143-7_25
14. Zhao, C., Zhang, N., Wang, H., Yang, B., Zhu, W., Li, Z., Zhu, M., Yin, S., Wei, S., Liu, L.: A compact and high-performance hardware architecture for crystals-dilithium. *IACR Transactions on Cryptographic Hardware and Embedded Systems* **2022**(1), 270–295 (2022). <https://doi.org/10.46586/tches.v2022.i1.270-295>